Time-reversible dissipative ergodic maps

William G. Hoover and Oyeon Kum
Department of Applied Science, University of California at Davis/Livermore and Lawrence Livermore National Laboratory, Livermore, California 94551-7808

Harald A. Posch
Institute for Experimental Physics, University of Vienna, Boltzmanngasse 5, Vienna A-1090, Austria
(Received 25 September 1995)

We construct especially simple families of piecewise-linear two-dimensional continuous maps. These maps generate sets of points resembling continuous dynamical trajectories sampled at discrete times. The generated sets of points share many properties with nonequilibrium many-body phase-space trajectories. These characteristic properties include (i) time reversibility, (ii) multifractal attractor-repellor pairs, and (iii) ergodicity, without stable fixed points or holes.

PACS number(s): 05.70.Ln, 11.30.Er, 47.70.−n

I. INTRODUCTION

Novel extensions of classical mechanics, which allow for thermodynamic and hydrodynamic dissipation while retaining time reversibility, have led to conceptual and computational advances in understanding and simulating a wide variety of nonequilibrium systems [1,2]. *Dissipation* is the inexorable conversion of work, or internal energy, to heat, as described by the second law of thermodynamics. *Time reversibility* implies that a movie of any developing system, projected backwards, still satisfies the same motion equations (but with the velocities reversed). Classical mechanics has been extended by incorporating special time-reversible constraint forces. These serve as sources or sinks of momentum and energy, and can also be used to enforce either instantaneous or time-averaged values of energy, temperature, stress, and the like for specified degrees of freedom. The feedback forces imposing these thermodynamic or hydrodynamic constraints on a system, though "artificial," provide the key to a theoretical understanding of systems both close to and far away from equilibrium.

The deterministic time-reversible nature of the underlying dynamical equations is firmly rooted in mechanics [3]. This reversibility property makes it possible to analyze the phase-space behavior of nonequilibrium steady states and to correlate their time-averaged macroscopic thermodynamic irreversible entropy production with their microscopic Lyapunov spectrum [4,5]. *Entropy production* is a measure of the rate at which work, or potential energy, is degraded to heat. The *Lyapunov spectrum* of Lyapunov exponents $\{\lambda\}$ describes the time-averaged orthogonal growths and decays, $\propto \{\langle e^{\lambda t}\rangle\}$ during a time t, of phase-space volume in the neighborhood of a typical phase-space trajectory.

A sufficiently long trajectory in n-dimensional phase space can be analyzed so as to determine all n of the Lyapunov exponents [1]. When at least one of these exponents is positive, signifying exponentially "sensitive dependence on initial conditions," the system is said to be *chaotic*. For stability, the sum of *all* the exponents must be negative or zero. In the *dissipative* case, which includes *all* nonequilibrium steady states, the sum of all the Lyapunov exponents is negative, signifying the collapse of the comoving phase-space volume onto (i) a fixed point, (ii) a limit cycle, or (iii) a strange attractor. The last of these possibilities occurs in the Lyapunov-unstable chaotic case. This case is the most interesting for physicists, who generate attractors as limit sets of long trajectories.

Chaotic attractors generated by time-reversible nonequilibrium dynamics are truly *strange*. On the one hand, they typically appear to be *ergodic*, with no holes [6], meaning that the system eventually, and even repeatedly, visits the neighborhood of every phase point in the n-dimensional space consistent with the dynamical conservation laws and any additional imposed constraints. The "Hausdorff dimension" D_H is the dimension of the space of the visited points.

On the other hand, the attractor points typically exhibit an "information dimension" D_I and a "correlation dimension" D_C, which are both strictly less than the constrained phase-space dimension: $D_H > D_I > D_C$. The information dimension characterizes the dependence of the occupation probability $\propto \delta^{D_I}$ of a typical phase-space hypercube, of sidelength δ, as is detailed in Sec. III. The correlation dimension describes the dependence of the number of pairs of attractor points lying at a distance δ of one another, $\propto \delta^{D_C}$. The limit set generated by the dynamics of our map is called an "attractor" to reflect the reduced dimensionality. All of the maps we study are, like the more complex Poincaré sections derived for physical systems, piecewise differentiable, in the sense that the Jacobians of the maps vary continuously in space. Though the combination of dissipation with ergodicity seems paradoxical, both numerical and theoretical investigations have established its reality.

Several mathematicians are making an effort to assimilate the paradoxical developments [7,8] by undertaking rigorous analytic studies of the chaotic nature of the continuous time-reversible thermostatted equations of motion. These workers have shown that many of the re-

sults established by numerical work a decade ago are rigorously true. There appears to a general consensus that the ergodic attractor, for the simple Galton Board problem described below, has an integral Hausdorff dimension and a smaller nonintegral information dimension, agreeing with the results of computer simulation [6]. Though the distinctions among the various fractal dimensions (capacity, Hausdorff, information, Kaplan-Yorke, correlation, etc.) are sometimes confused in the literature, there appears to be no real doubt that the two approaches, theoretical and numerical, are close to providing a common understanding of the irreversibility exhibited by time-reversible systems.

With the present work we hope to make the nature of irreversible physical systems clearer and more accessible to mathematicians, as well as to physicists interested in the fundamentals of simulation, by relating typical features of the solutions of the differential motion equations to phase-space structures generated by continuous maps. The idea of simplifying dynamical analyses by forming such maps, projecting orbits onto a phase-space hyperplane, a *Poincaré plane,* is a century old. Even though the complete Lyapunov spectra of many-dimensional multifractal objects can be analyzed numerically for systems of a few hundred degrees of freedom [9,10], the simplification obtained by reducing the dimensionality from a three-dimensional continuous flow to a two-dimensional map remains real and important for analytic work.

The aspects of nonequilibrium systems that we wish to emphasize have previously been illustrated by the Galton board example [1,4,6–8,11]. This system is arguably the simplest known ergodic nonequilibrium system. It consists of a single point particle, driven through an infinitely periodic "triangular lattice" of hard-disk scatterers by a constant accelerating field. The lattice of scatterers has hexagonal symmetry, with each scattering disk having six similar neighbors, located at the vertices of a regular hexagon. The overall density of the scattering lattice must be sufficiently dense to ensure collisions with the moving particle. A stationary strange attractor results when a time-reversible constraint force is used to keep the kinetic energy of the driven particle fixed. In the absence of such an energy constraint the moving particle cannot achieve a stationary state.

The Galton board problem was first analyzed in terms of (fairly complicated) maps [11–13]. It displays the three typical features many physicists associate with large nonequilibrium systems:

(i) time-reversible equations of motion;
(ii) multifractal repellor→attractor pairs;
(iii) ergodic phase-space structures with no stable fixed points.

With time-reversible dynamics the phase-space *repellor* is the time-reversed image of the strange attractor. The repellor is a "source" of the flow in the same sense that the attractor is a "sink." Both objects have a singular probability density, with the probability of occupying a small region in phase space varying as a fractional power of the region's size. When the probability power law additionally varies from point to point, the distribution is said to be *multifractal.*

An *ergodic* phase-space flow links all the repellor states (occupied in the distant past) to the geometrically similar attractor states (to be occupied in the distant future) through trajectories that come arbitrarily close to all allowed phase-space points. Both time reversibility and the existence of an attractor-repellor pair are quite unusual properties for maps [14]. It is our purpose to explore the degree to which all three of the properties above can be realized in two-dimensional *deterministic* (one-to-one) time-reversible maps with simple structures.

The well-known baker, Bernoulli, and Arnold cat maps are *not time reversible* in the sense that we use these words, though mathematicians have broadened the definition of reversibility to include at least the baker and cat maps [14]. Also not reversible are the *millions* of polynomial maps studied by Sprott [15–18]. Our definition of reversibility is a relatively rare attribute of maps. It requires two or more dimensions, is relatively difficult to analyze, and has relatively rarely been discussed [14]. We begin by requiring that, like Einstein's, Maxwell's, Newton's, and Schrödinger's equations, time-reversible mapping equations, implemented in going forward in time, must be *identical* to those required to go backward in time along the same space trajectory. Thus neither of the baker maps, with horizontal cuts and vertical displacements or with vertical cuts and horizontal displacements, is time reversible. The details of both types of baker map dynamics are outlined in Fig. 1.

It should be noted that some prefer a definition of reversibility that allows combinations of reflections, inversions, or rotation in the phase space, called involutions, in comparing the forward and backward evolutions of a system. For details see Ref. [14].

Real nonequilibrium systems involve *dissipation,* the irreversible conversion of work, or internal energy, into heat. Theoretical models for dissipative systems usually

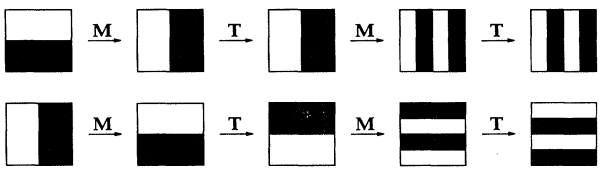

FIG. 1. The operations **TMTM**, applied to either of two versions of the baker map, are equivalent to two forward iterations of the corresponding map. Two more iterations of that map, "backward" in time, would just continue the process of division. The inverses of these baker maps differ from the maps themselves, so that these maps are not time-reversible. Notice that in the top "horizontal-cut" baker map, the bottom half of the square becomes the right half after mapping **M** is applied. In the lower "vertical-cut" baker map (which *is* the inverse $\mathbf{M}^{-1}$ of the top map), the right half of the square becomes the bottom half. In either case the time-reversal operation **T** corresponds to a reflection about the horizontal midplane.

incorporate frictional forces, which cause a shrinkage of available phase-space states as times goes on. The damped harmonic oscillator, which approaches the fixed point ($q=0, p=0$), is the most familiar example.

In the continuous case, time-reversible dissipation *is* possible, as the Galton board example [6–8,11,19] establishes. This example is prototypical of nonequilibrium systems in that the phase-space flow links together an unstable multifractal repellor source to a geometrically similar, but stable, strange attractor sink. It was the mathematical complexity of the solution process for the Galton board example that led us to consider the simpler maps of the present work. We show here that these maps generate attractor-repellor pairs, just as do their continuous relatives.

The last generic property of nonequilibrium systems we wish to discuss is the simultaneous presence of ergodicity—the periodic visiting of *all* phase points, arbitrarily closely—and dissipation—the shrinking of the comoving phase volume. This combination seems paradoxical. Ergodicity strongly suggests that the dynamics cannot incorporate the shrinkage necessary to progress toward a fractal object. In fact, such progress is obviously impossible in a discrete space with a finite number of state points. In such a discrete case, any ergodic deterministic trajectory must necessarily be periodic in time, and must therefore lack the shrinking associated with dissipation.

This short paper is arranged as follows: some definitions, together with discussion, of time-reversible maps, make up Sec. II; a realistic demonstration of time-reversible dissipation, based on simple time-reversible combination maps, follows in Sec. III; finally, we discuss our results and conclusions in Sec. IV.

II. TIME-REVERSIBLE TWO-DIMENSIONAL MAPS

We consider here two-dimensional piecewise-continuous maps $\{\mathbf{M}\}$, which generate new coordinates $\mathbf{r}'$ from old ones, $\mathbf{r}'=\mathbf{r}'(\mathbf{r})=\mathbf{M}(\mathbf{r})$. For simplicity and convenience, both $\mathbf{r}$ and its mapped image $\mathbf{r}'$ are restricted to lie within a periodic unit square centered on the origin:

$$-0.5<x\rightarrow x'<+0.5\ ,\quad -0.5<y\rightarrow y'<+0.5\ .$$

We think of the Cartesian components of $\mathbf{r}=(x,y)$ as representing a *coordinate* x and a *momentum* y (with the momentum changing sign, $+y\rightarrow -y$, in a time-reversed motion). Thus our Cartesian space is a caricature of classical phase space and our maps are caricatures of equations of motion.

Evidently a single-valued deterministic map $\mathbf{M}$ operating on (x,y) produces a new pair of coordinates (x',y'), which can be viewed as representing the next point along a finite-time-difference phase-space trajectory or else the next intersection of such a trajectory with a Poincaré plane. The inverse of $\mathbf{M}$, denoted $\mathbf{M}^{-1}$, would produce the pair (x,y) from the pair (x',y'). To define and discuss time reversibility, we need also to define separately a *time-reversal map* $\mathbf{T}$. $\mathbf{T}$ does nothing more than change the sign of the momentumlike coordinate y: $+y\rightarrow -y$. $\mathbf{T}$ is thus its own inverse: $\mathbf{T}\mathbf{T}^{-1}=\mathbf{T}\mathbf{T}\equiv\mathbf{I}$, where $\mathbf{I}$ is the identity map.

The concept of time reversibility [1,2,7,14], in the restricted use we apply throughout this paper, can now be expressed in terms of the one-to-one maps $\mathbf{M}$ and $\mathbf{T}$ and the phase-space coordinate-momentum pairs (x,y). *A map* $\mathbf{M}$ *is said to be time reversible if and only if it satisfies the identity*

$$(x,y)=\mathbf{TMTM}(x,y)\ . \tag{1}$$

The maps are applied from right to left in this definition, first $\mathbf{M}$, then $\mathbf{T}$, then $\mathbf{M}$ again, and finally $\mathbf{T}$ again. The first of *two* occurrences of the time-reversal map corresponds to a first time reversal at (x',y'), giving $(x',-y')$. The second reversal occurs after the map $\mathbf{M}$ returns the trajectory from $(x',-y')$ to $(x,-y)$. From this definition, it follows also that the inverse of $\mathbf{M}$, $\mathbf{M}^{-1}$, is given by another time-symmetric map

$$\mathbf{M}^{-1}=\mathbf{TMT}\ .$$

Figure 2 illustrates the basic cycle of four operations in [1] for the two-dimensional map corresponding to the phase-space dynamics of a one-dimensional harmonic oscillator of unit frequency. The map $\mathbf{M}$, which advances the coordinate-momentum pair forward in time (clockwise in phase space) by Δt, is the transpose of a (counterclockwise) rotation matrix:

$$\mathbf{M}=\begin{bmatrix}+\cos\Delta t & +\sin\Delta t\\ -\sin\Delta t & +\cos\Delta t\end{bmatrix}\ .$$

The defining equation (1) is conceptually complicated, and therefore of little use, in the direct construction of time-reversible maps. It does provide a useful method for

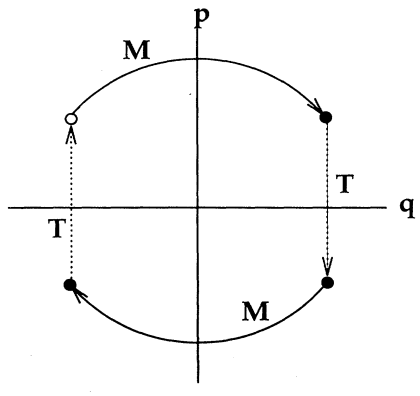

FIG. 2. The operations **TMTM**, applied to a one-dimensional oscillator, initially located at the open-circle point $(q,p)=(-\delta,+\delta)$. The motion map $\mathbf{M}$ advances the oscillator "trajectory" through a quarter period to the new point $(+\delta,+\delta)$. Then, the time-reversal map $\mathbf{T}$ reverses the momentum from $+\delta$ to $-\delta$, with no coordinate change. A second application of the motion map carries the point $(+\delta,-\delta)$ to $(-\delta,-\delta)$, where a final time-reversal of the momentum regenerates the initial state.

checking solutions. Intuition, though slow, proved to be the most effective tool in finding interesting solutions of the equation. In retrospect, it is possible to motivate the generation of the solutions found in this way. Such a constructive approach begins by considering the simplest (homogeneous) transformations of two-dimensional space into itself and checking these for time reversibility, in the sense incorporating the **T** map equation (1) above. Consider the simplest useful examples, taken from the two macroscopic hydrodynamic shear flows:

$$u_x = \dot{\varepsilon} y \ , \quad u_y = \dot{\varepsilon} x \ .$$

In these flows **u** is velocity and $\dot{\varepsilon}$ is the strain rate. In converting these hydrodynamic flows to Cartesian maps, we use periodic boundaries to confine the displaced variables to the unit square.

The first of these area-preserving finite-shear examples we call **X**,

$$\mathbf{X}: \ x \to x' = x + \varepsilon y \ , \quad y \to y' = y \ ,$$

including, if necessary, the addition or subtraction of 1.0 to the new coordinate x' to ensure that its position lies within the unit square. This map is clearly linear and time reversible, as is illustrated in Fig. 3. The simple shear transformation by itself is certainly far from being either ergodic or mixing because the y coordinate never changes. On the other hand, a *symmetric* combination of two linear maps, using the corresponding vertical displacements from **Y**,

$$\mathbf{Y}: \ x \to x' = x \ , \quad y \to y' = y + \varepsilon x \ ,$$

can be used to make the time-reversible combination deformation **XYX**. By contrast, the Arnold cat map, **XY**, with $\varepsilon = 1$, is not time reversible. In the absence of periodic boundaries **XYX** carries the unit square into a long, thin parallelogram. Because the motion expands in the direction of the longer diagonal of the parallelogram and contracts in the perpendicular direction, the result is a linear hyperbolic map [12]. Unless peculiar zero-measure initial conditions are chosen, this map is ergodic and mixing.

Given that both **X** and **Y** are reversible maps, the time reversibility of the symmetric combinations **XYX** and **YXY**, according to (1), follows easily from the self-inverse property of **T**:

$$\mathbf{TXYXTXYX} = \mathbf{TXYT}^{-1}\mathbf{YX} = \mathbf{TXYTYX} = \mathbf{TXT}^{-1}\mathbf{X}$$
$$= \mathbf{TXTX} \equiv \mathbf{I} \ .$$

Thus, unlike either of the asymmetric map combinations **XY** or **YX**, the compound maps **XYX** or **YXY** are not only time reversible but also, like the cat map, ergodic (for nearly all initial conditions), due to the loss of coherence in both the horizontal and vertical directions. These compound maps do, however, provide no possibility for phase-space density change and so are not at all characteristic of the microscopic dynamic motion equations.

To provide this possibility, we define and use another transformation **P**, which is also illustrated in Fig. 3. **P** corresponds to the simultaneous proportional reflection of both the x and y coordinates in mirrors located at $\pm m$. An x coordinate lying between 0 and a reflecting mirror at $\frac{1}{3}$, for example, provide a new coordinate x' between $\frac{1}{3}$ and $\frac{1}{2}$, while a coordinate between $\frac{1}{3}$ and $\frac{1}{2}$ is mapped to the interval between 0 and $\frac{1}{3}$. For positive x, and a mirror at $0 < m < \frac{1}{2}$, the mapping $\mathbf{P}$: $x_{\text{left}} \leftrightarrow x_{\text{right}}$, which is its own inverse, links together two x coordinates according to a simple linear relation:

$$(x_{\text{right}} - m)/(x_{\text{left}} - m) = (2m-1)/2m \ .$$

Negative x, as well as the y coordinates, are treated similarly by **P**. For choices of m other than the area-preserving value of $\frac{1}{4}$, this map contains both expanding and contracting regions and so has the potential to produce a multifractal attractor-repellor pair.

The combination **XPYPX** turns out to be time reversible, mixing, and to have no stable fixed points. Strong empirical evidence for ergodicity can easily be obtained by iterating this map, using a fast computer and noting the independence of the statistical results obtained to the chosen initial point. The $\{(x,y)\}$ pairs so generated can be used to compute both (i) the occupation probabilities within a network of small squares and (ii) all of the vari-

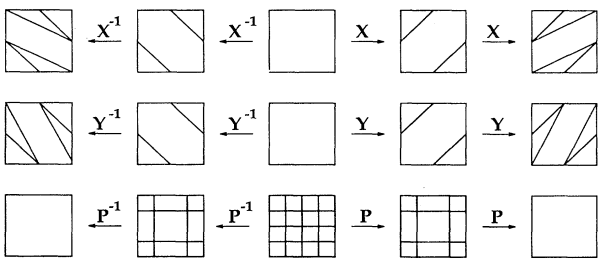

FIG. 3. The three time-reversible transformations, carried forward and backward in time for two iterations, of the corresponding maps (**X**,**Y**,**P**). Compare with the Galton board maps illustrated on p. 281 of Ref. [1].

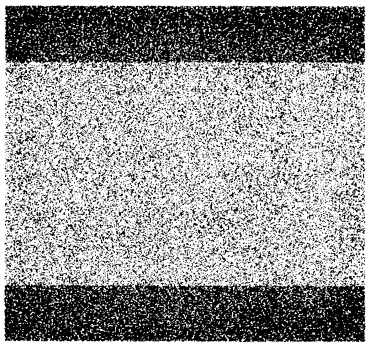

FIG. 4. 100 000 points generated by iterating the map **XPYPX**, where $m = \frac{1}{3}$, starting at the (arbitrary) (x,y) point (0.3,0.4). The information dimension of this ergodic attractor is 1.94.

ous fractal dimensions [6,12,13]. See Fig. 4 for the result of 100 000 iterations of this map with $m=\frac{1}{3}$. Many other combination maps, formed from time-symmetric sequences of the $\{\mathbf{X},\mathbf{Y},\mathbf{P}\}$ operations, have these same properties, as would additional maps containing other simple time-reversible geometric operations, such as rotations and reflections.

The small catalog of simple maps discussed so far $\{\mathbf{X},\mathbf{Y},\mathbf{P}(m)\}$ turns out to be fully sufficient to replicate all the qualitative behavior found in the time-reversible, but dissipative, systems studied with nonequilibrium molecular dynamics [1,2,4–11]. We consider in more detail some simple specific examples in the following section.

III. CONSTRUCTING TIME-REVERSIBLE DISSIPATIVE MAPS

Neither the homogeneous linear shear maps **X** and **Y** nor the inhomogeneous bilinear $\mathbf{P}(m)$ maps are by themselves capable of representing the dissipative systems treated in nonequilibrium simulations. Maps representative of realistic systems have to combine the shear exhibited by **X** and **Y** with the expansion and contraction inherent in **P**. In dynamical systems, it is heat exchange, through boundary energy or temperature constraints, that causes the comoving phase-space volume to expand or contract, with the generic consequence that attraction—onto a "strange attractor"—eventually wins out [1,2,4–6]. It is characteristic of nonequilibrium simulations that close to equilibrium, where the dissipation is second order in the magnitude of the deviation, the attractor's information and correlation dimensions approach close to the Hausdorff and embedding dimensions, with the dimensionality difference varying as the square of the deviation from equilibrium [6–8,19]. For our maps the embedding and Hausdorff dimensions appear to be exactly the same. Most known maps, however, provide fractal dimensions, both Hausdorff and information, very far from the embedding dimension [12–18].

Apart from a fixed point at the origin, the linear shear maps considered in Sec. II can easily provide an ergodic coverage of the unit square. The special case **XYYX**, with unit strains

$$\mathbf{X}\colon (x'=x+y\ ;y'=y)\ ,\quad \mathbf{Y}\colon (x'=x\ ;y'=x+y)\ ,$$

apparently provides uniform coverage of the unit square. See Fig. 5. Though this figure, as well as Figs. 4 and 6, was generated by iterating a single initial condition forward in time, we carefully verified that, apart from isolated unstable periodic orbits, the results are statistically (i) independent of the chosen initial point and further (ii) indistinguishable from limit sets generated by iterating initial ensembles of thousands of randomly chosen, or ordered, points.

Many combinations of the three maps so far considered $\{\mathbf{X},\mathbf{Y},\mathbf{P}(m)\}$ apparently have *all* the properties typical of nonequilibrium dynamical systems. Such combinations can be generated and evaluated on a modern workstation, in a way pioneered by Sprott [15–17], by combining thousands of symmetrized sequences of such maps and then generating a few tens of thousands of points for each such map, selecting those with interesting properties for subsequent visual display and evaluation. Reasonably long time-reversible sequences, composed of time-reversible maps, such as

$$\mathbf{M}_1\mathbf{M}_2\mathbf{M}_3\mathbf{M}_4\mathbf{M}_3\mathbf{M}_2\mathbf{M}_1$$

can be used, where the sets of all such participating time-reversible maps $\{\mathbf{M}_1,\mathbf{M}_2,\mathbf{M}_3,\mathbf{M}_4\}$ can be chosen exhaustively.

Consider the dissipative collapse of phase-space probability to a "multifractal" attractor. Such behavior has been shown to characterize the Galton board [1,6–8,11] and many other nonequilibrium systems [1,2], and is by now expected to be generic for many-body systems of interest in nonequilibrium statistical mechanics. The collapse onto a multifractal phase-space attractor sink (while simultaneously fleeing from a congruently similar repellor

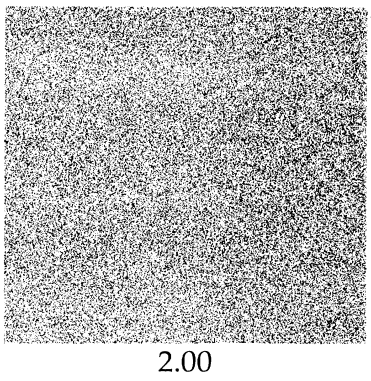

FIG. 5. 100 000 points generated by iterating the map **XYYX**, starting at the (arbitrary) (x,y) point (0.3, 0.4) and using unit strain, $\varepsilon\equiv 1$. The information dimension of the map is 2.00. **YXXY** produces a similar map.

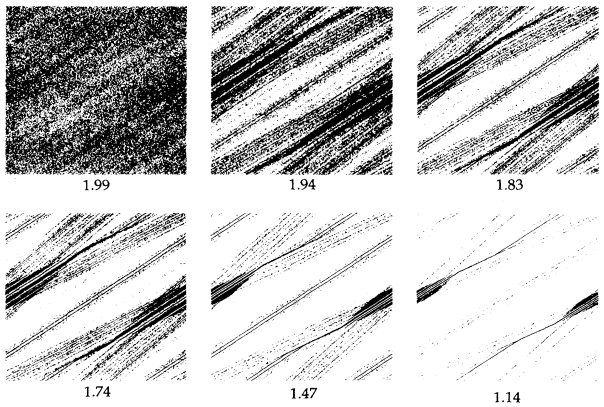

FIG. 6. Point distributions generated by iterating the map **XYPYX**, where the values of the information dimension D_I, ranging downward from 1.99 to 1.14, are indicated on the distributions. The corresponding Δm values are 0.01, 0.05, 1/12, 0.10, 0.15, and 0.17.

source) *can* occur if the dynamic probability redistribution is sufficiently nonlinear. In a *multifractal* attractor the power-law dependence of the phase-space measure μ on the grid spacing δ used to measure it varies from point to point.

We can check for the characteristic multifractal character of nonequilibrium probability densities by simultaneously measuring the Hausdorff, information, and correlation dimensions D_H, D_I, and D_C. These generally differ [6,7,12,13]. The information dimension [12,13] describes the way in which the phase-space measure diverges as the grid spacing δ used to determine the measure approaches zero:

$$\langle \ln\mu \rangle_\delta \equiv \sum (N_k/N)\ln(N_k/N) \approx D_I \ln\delta + O(1) + \cdots .$$

This definition coincides with the intuitive notion of dimension if one imagines the uniform case in which all the N_k have the average value, $N_k = N\delta^2$, for the unit square. Accurate estimates for D_H, D_I, and D_C require that the mean value of the cell occupation numbers greatly exceeds unity.

We noted first that **XYYX** and **YXXY** are useful maps for generating the homogeneous ergodic density analogous to equilibrium. Iterated 100 000 times, these combination maps typically provide estimates for D_I lying within 0.01 of 2.00 if 32^2 or 64^2 cells are used. Adding the nonlinear **P**(m) map provides a family of strange attractors, of which typical representatives are shown in Fig. 6. The corresponding repellors are the time-reversed images of these attractors. The maps have information dimensions that decrease quadratically from 2 as m is increased or decreased away from the equilibrium value, $m = \frac{1}{4}$. Figure 7 presents convincing evidence for this functional form, and indicates as well a transition region in the vicinity of $\Delta m \equiv 0.25 - m \approx 0.15$. For $\Delta m > 0.17$ the ergodic phase-space distribution becomes replaced by limit cycles analogous to those found in high-field Galton board dynamics.

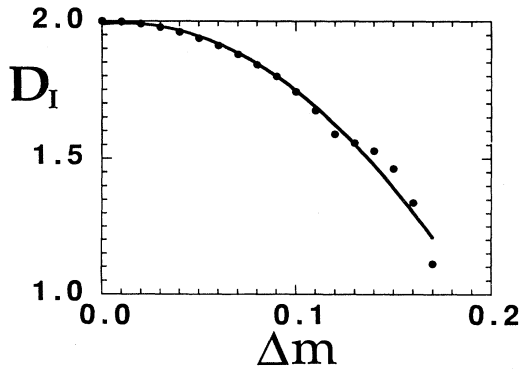

FIG. 7. Dependence of the information dimension D_I on Δm, the offset of m from the equilibrium value $m = \frac{1}{4}$. The smooth quadratic portion of the curve corresponds to the ergodic attractors of Fig. 6. In this region the **XYPYX** map has eight unstable fixed points. For larger values of $\Delta m = 0.25 - m$ than are shown here, the corresponding maps give limit cycles.

Thus, by combining homogeneous linear shears with an inhomogeneous time-reversible and dissipative (locally non-area-conserving) map, we have succeeded in simulating all the properties of a typical nonequilibrium system. It is reasonable to expect that the mathematical theory of these piecewise-linear time-reversible maps is more amenable to analysis than are the original nonlinear differential equations of nonequilibrium molecular dynamics.

IV. CONCLUSIONS

The main product of our exploratory investigations is the simple set of linear time-reversible maps {**X**,**Y**,**P**}, which can be combined to give rise to the same generic behavior observed in solving the differential motion equations of nonequilibrium molecular dynamics. Figures 6 and 7 show that we have reached our goal of producing a simple combination map with the same topological properties as the relatively complicated map characterizing the Galton board.

Because the underlying hard-disk dynamics in the Galton board is impulsive, the corresponding phase-space motion contains bifurcations, in which nearby trajectories separate discontinuously. For this reason the smooth "Smale horseshoe" deformation, resulting from the stretching and bending associated with continuous forces, is absent here. Such a bending deformation can be described by a quadratic map [12,13]. We expect that time-reversible quadratic maps could also be constructed. The simplest way would be to extend the linear deformations used here (corresponding to the isoperimetric Lagrange-polynomial mappings of continuum mechanics) so as to describe *quadratic* deformations within contiguous hexagonal regions. The six coefficients in the corresponding quadratic forms $\{a + bx + cy + dx^2 + exy + fy^2\}$ can be fitted to six conditions at the hexagon vertices.

The dissipation (contraction to a multifractal attractor) found here, as well as in time-reversible many-body systems, appears at first to be as paradoxical as Boltzmann's H theorem derivation of macroscopic irreversible behavior from microscopic reversible motion equations. It certainly is odd that time-reversible ergodic equations of motion can simultaneously provide the shrinking of phase-space volume typical of dissipation, along with an ergodic development that repeatedly visits all regions of a continuous space. This paradoxical behavior may well reflect the mysterious paradoxes [20] that are inherent in the concept of a continuum.

The simple time-reversible maps found here parallel equilibrium and nonequilibrium molecular dynamics. Now that a rigorous understanding of the simplest dynamical models is available, the new reversible ergodic maps should provide a simpler, mathematically more tractable link between the two fields. The paradoxical

TABLE I. Fully converged Lyapunov exponents and the corresponding Kaplan-Yorke dimensions.

Δm	λ_1	λ_2	D_{KY}
0.00	1.763	−1.763	2.000
0.01	1.761	−1.768	1.996
0.05	1.717	−1.881	1.913
1/12	1.614	−2.082	1.775
0.10	1.523	−2.210	1.689
0.15	1.155	−2.611	1.442
0.17	0.534	−3.161	1.169

finding that continuum phase spaces can simultaneously support dissipation and ergodicity has here been extended, computationally, to time-reversible maps, which should provide a simpler interpretation of this fundamental property of nonequilibrium systems. We expect that these new models, and their variants, will prove useful to a variety of projects devoted to the understanding of irreversibility.

In obtaining these results, progress would have been much slower without a fast graphics workstation. One can only wonder what the reactions of Poincaré and of Boltzmann to the new possibilities of graphic displays would be.

More elaborate calculations than those in the text (with billions of points and millions of bins) were carrried out, but failed to reduce the uncertainties in the information dimensions given in Fig. 6 below about 0.01. Fully converged Lyapunov exponents, and the corresponding Kaplan-Yorke dimensions, appear in Table. I.

ACKNOWLEDGMENTS

This work was supported, in part, by the Lawrence Livermore National Laboratory, under the auspices of the U. S. Department of Energy, through Contract No. W-7405-Eng-48; in part, by a grant from the Agency for Defense Development, Republic of Korea; and, in part, through an Interuniversity Transfer Agreement for the support of Oyeon Kum. Carol Hoover, John Roberts, Clint Sprott, and Bill Vance provided a variety of very helpful comments and suggestions. We especially thank Joel Lebowitz for his comments concerning Ref. [8].

[1] W. G. Hoover, *Computational Statistical Mechanics* (Elsevier, Amsterdam, 1991).
[2] D. J. Evans and G. P. Morriss, *Nonequilibrium Liquids* (Academic, New York, 1990).
[3] W. G. Hoover, Phys. Lett. A **204**, 133 (1995).
[4] B. L. Holian, W. G. Hoover, and H. A. Posch, Phys. Rev. Lett. **59**, 10 (1987).
[5] E. G. D. Cohen, Physica A **213**, 293 (1995). This is a comprehensive review of our work.
[6] W. G. Hoover and B. Moran, Phys. Rev. A **40**, 5319 (1989).
[7] W. N. Vance, Phys. Rev. Lett. **69**, 1356 (1992).
[8] N. I. Chernov, G. L. Eyink, J. L. Lebowitz, and Y. G. Sinai, Phys. Rev. Lett. **70**, 2209 (1993).
[9] W. G. Hoover and H. A. Posch, Phys. Rev. E **51**, 273 (1995).
[10] H. A. Posch, W. G. Hoover, and O. Kum, Phys. Rev. E **52**, 1711 (1995).
[11] B. Moran, W. G. Hoover, and S. Bestiale, J. Stat. Phys. **48**, 709 (1987).
[12] For many examples of maps and fractals, see M. Schroeder, *Fractals, Chaos, Power Laws* (Freeman, New York, 1991), and Ref. [13].
[13] H. G. Schuster, *Deterministic Chaos, An Introduction* (VCH, Weinheim, 1988).
[14] J. A. G. Roberts and G. R. W. Quispel, Phys. Rep. **216**, 63 (1992).
[15] J. C. Sprott, Phys. Lett. A **173**, 21 (1993).
[16] J. C. Sprott, Phys. Rev. E **50**, 647 (1994).
[17] J. C. Sprott, Phys. Lett. A **192**, 355 (1994).
[18] W. G. Hoover, Phys. Rev. E **51**, 759 (1995).
[19] C. Dellago and H. A. Posch, Phys. Rev. E **52**, 2410 (1995).
[20] R. M. French, Math. Intell. **10** (4), 21 (1988).

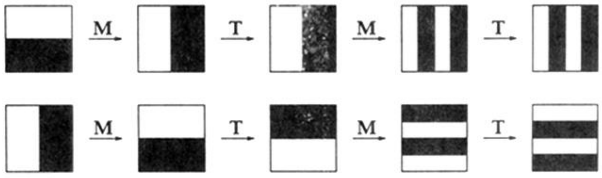

FIG. 1. The operations **TMTM**, applied to either of two versions of the baker map, are equivalent to two forward iterations of the corresponding map. Two more iterations of that map, "backward" in time, would just continue the process of division. The inverses of these baker maps differ from the maps themselves, so that these maps are not time-reversible. Notice that in the top "horizontal-cut" baker map, the bottom half of the square becomes the right half after mapping **M** is applied. In the lower "vertical-cut" baker map (which *is* the inverse $\mathbf{M}^{-1}$ of the top map), the right half of the square becomes the bottom half. In either case the time-reversal operation **T** corresponds to a reflection about the horizontal midplane.

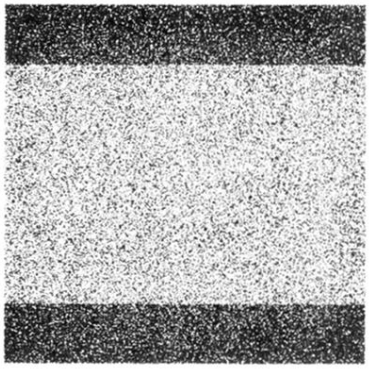

FIG. 4. 100 000 points generated by iterating the map **XPYPX**, where $m = \frac{1}{3}$, starting at the (arbitrary) (x,y) point (0.3,0.4). The information dimension of this ergodic attractor is 1.94.

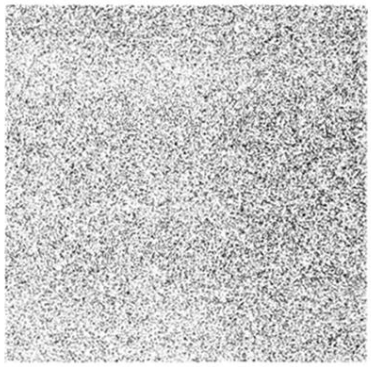

2.00

FIG. 5. 100 000 points generated by iterating the map **XYYX**, starting at the (arbitrary) (x,y) point (0.3, 0.4) and using unit strain, $\varepsilon \equiv 1$. The information dimension of the map is 2.00. **YXXY** produces a similar map.

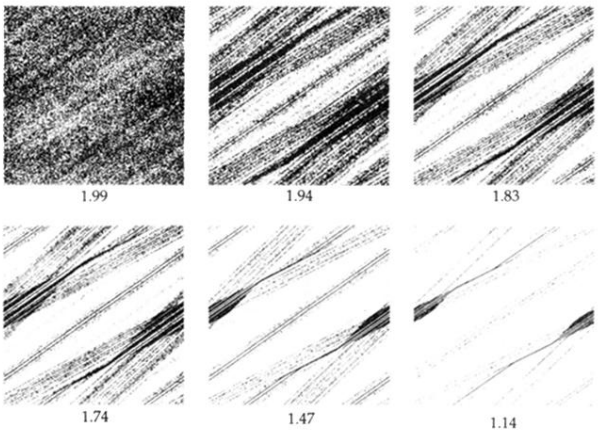

FIG. 6. Point distributions generated by iterating the map **XYPYX**, where the values of the information dimension D_I, ranging downward from 1.99 to 1.14, are indicated on the distributions. The corresponding Δm values are 0.01, 0.05, 1/12, 0.10, 0.15, and 0.17.